

Colicin E1 opens its hinge to plug TolC

Authors: S. Jimmy Budiardjo¹, Jacqueline J. Stevens², Anna L. Calkins³, Ayotunde P. Ikujuni², Virangika K. Wimalasena², Emre Firlar⁴, David A. Case⁵, Julie S. Biteen³, Jason T. Kaelber⁴ and Joanna S.G. Slusky^{1,2,*}

Affiliations:

¹ Center for Computational Biology, The University of Kansas, 2030 Becker Dr., Lawrence, KS 66047

² Department of Molecular Biosciences, The University of Kansas, 1200 Sunnyside Ave. Lawrence KS 66045

³ Department of Chemistry, University of Michigan, Ann Arbor MI 48109-1055.

⁴ Rutgers CryoEM & Nanoimaging Facility and Institute for Quantitative Biomedicine, Rutgers, The State University of New Jersey, Piscataway, NJ 08854, USA

⁵ Department of Chemistry and Chemical Biology, Rutgers University, Piscataway, NJ 08854 USA

*Correspondence: slusky@ku.edu.

ABSTRACT

The double membrane architecture of Gram-negative bacteria forms a barrier that is effectively impermeable to extracellular threats. Bacteriocin proteins evolved to exploit the accessible, surface-exposed proteins embedded in the outer membrane to deliver cytotoxic cargo. Colicin E1 is a bacteriocin produced by, and lethal to, *Escherichia coli* that hijacks the outer membrane proteins TolC and BtuB to enter the cell. Here we capture the colicin E1 translocation domain inside its membrane receptor, TolC, by high-resolution cryoEM. Colicin E1 binds stably to TolC as an open hinge through the TolC pore—an architectural rearrangement from colicin E1's unbound conformation. This binding is stable in live *E. coli* cells as indicated by single-molecule fluorescence microscopy. Finally, colicin E1 fragments binding to TolC plugs the channel,

29 inhibiting its native efflux function as an antibiotic efflux pump and heightening susceptibility to
30 four antibiotic classes. In addition to demonstrating that these protein fragments are useful
31 starting points for developing novel antibiotic potentiators, the known variety of other colicin-
32 binding partners will allow our method to inhibit other outer membrane protein functions.

33

34 INTRODUCTION

35 In Gram-negative bacteria, the concentric structures of the outer membrane, cell wall, and
36 cytoplasmic membrane protect the cell from extracellular threats. Of these protective structures,
37 the outer membrane forms a particularly formidable barrier⁵, owing to the impermeability of the
38 lipopolysaccharide (LPS) layer that constitutes the outer membrane⁷. The primary means by
39 which external molecules can gain access to the cell is through the ~100 varieties of barrel-
40 shaped proteins that are embedded in each bacterium outer membrane⁸ and whose diverse
41 functions include the transport of molecules across the membrane—specifically, the import of
42 nutrients and metabolites and the export of toxins and waste.

43 Because outer membrane proteins (OMPs) are accessible from outside the cell,
44 bacteriophage and bacterial toxins have evolved to exploit OMPs to initiate delivering cargo
45 across the outer membrane. Bacteriocins hijack the OMPs of a target bacterium to cross its
46 impermeable outer membrane and kill the bacterium. Colicins are *E. coli*-specific bacteriocins,
47 protein toxin systems through which bacteria engage in bacterial warfare with other, similar
48 bacteria. Although colicins differ in their receptor targets and killing mechanisms, most colicins
49 share a common tri-domain architecture, comprising the following components: (i) an N-terminal
50 translocation (T) domain, (ii) a receptor-binding (R) domain, and (iii) a C-terminal cytotoxic (C)
51 domain (Figure 1A). Much of what is known of *E. coli* colicin import has been determined through
52 studies of the colicin E3 and E9 as reviewed by Cramer et al.⁹ Import is initialized by R domain

53 binding to the vitamin B12 transporter, BtuB, with high affinity^{10,11}; this binding localizes the
54 colicin onto the outer membrane. Once the colicin is tethered to the outer membrane surface, the
55 T domain initiates translocation using the secondary OMP receptor OmpF to access TolA/Pal
56 system for group A colicins or the Ton system group B colicins. In most cases, the T domain
57 requires an OMP distinct from the R domain target.¹² A handful of colicins have been
58 structurally characterized with their OMP counterparts, although not in their entirety. Previous
59 structures of short N-terminal fragments of the T domain of ColE9 with OmpF¹³ and the The R
60 domains of ColE2/E3 and Ia with BtuB^{11,14} and Cir¹⁰, respectively showed that T domains fully
61 penetrate deeply into lumen of the outer membrane receptors while R domains interact with the
62 extracellular loop regions of their receptors. Studies of the bacteriocin pyocin S5 from
63 *Pseudomonas aeruginosa* suggest that bacteriocin architectures and mechanisms may be
64 conserved across all Gram-negative species.

65 Colicin E1 is a bacteriocin secreted by *E. coli* that enters the periplasm of neighboring
66 cells and forms a pore on the cytoplasmic membrane leading to membrane depolarization and
67 cell death. Colicin E1 uses TolC, the outer membrane component of the acridine efflux pump, as
68 the T domain receptor¹⁵ and BtuB as the R domain receptor¹⁶. A high-resolution x-ray structure
69 exists of only the cytotoxic domain of colicin E1¹⁷ but not the T or R domains, thus no
70 mechanistic insights can be gained about initial steps of import. Domain swapping experiments
71 between colicin A and E1 identified regions of the protein that interact with specific outer
72 membrane proteins. Early studies of pore forming colicins, including E1, showed that cytotoxic-
73 domain-induced K⁺ efflux on the inner membrane can be reversed after it has begun by
74 subsequent addition of trypsin to cells. This, in addition to trypsin's inability to cross the outer

75 membrane, led to the belief that portions of colicin remain tethered to their OMP partners as the
76 cytotoxic domain depolarizes the cytoplasmic membrane.¹⁸⁻²¹

77 In order to understand the early stages of colicin E1 import, functional studies of
78 truncations of colicin E1 which lack the cytotoxic domain have been characterized *in vitro*.
79 Residues 100-120 of colicin E1 (termed the ‘TolC box’, Figure 1A) have been shown to be
80 necessary but not sufficient for binding TolC. Peptides that include the TolC box co-elute with
81 TolC²² and disrupt channel conductance^{22,23}. Moreover, *E. coli* exposure to TolC-box-containing
82 peptides can prevent subsequent binding and cytotoxicity of full-length colicin E1²⁴. Circular
83 dichroism of the T domain indicates that it exists as a helical hairpin (closed hinge) in solution
84 similar to other colicin T domains²⁵ and that the proline at the center of the TolC box forms its
85 apex²². This measurement led to the proposal, known as the “pillar model,”²² that the T domain
86 inserts into the TolC barrel as a helical hairpin where the N and C-termini are pointing to the cell
87 exterior. According to this model, the hairpin stuck in TolC acts as a buttress to facilitate the
88 cytotoxic domain entry directly through the membrane.

89 A competing model for colicin E1 import, known as the “total thread” model^{9,22}, posits
90 that the protein unfolds and passes through TolC N-terminus-first as an unstructured peptide,
91 followed by refolding in the periplasm. In this model the binding between the intrinsically
92 unstructured colicin N-termini and periplasmic proteins^{24,26} creates a pulling force that results in
93 the translocation of the whole colicin.

94 Here we use cryogenic electron microscopy (cryoEM) to solve the high-resolution
95 structure of the colicin E1 T domain bound to TolC. We find that colicin E1 binds stably to
96 TolC, not as a helical hairpin but as a single-pass folded helix with the N-terminus inside the
97 periplasm. Additionally, we find that the colE1 TR domain binds TolC *in vivo* as well. Using

98 single-molecule fluorescence microscopy, we find that colE1-TR, lacking the cytotoxic domain,
99 remains stalled on the outer membrane and does not fully translocate into cells. Lastly, we
100 leverage this stalling of ColE1 to block the native TolC function as an antibiotic efflux pump.
101 Because they are accessible from outside the cell, OMPs are attractive targets for the
102 development of novel antibiotics, and research has begun to reveal the therapeutic potential of
103 interfering with OMP structure and function. Recently, a monoclonal antibody was found to
104 inhibit OMP folding with bactericidal effects²⁷.

105 Here by determining the structure and mechanism of colE1 insertion we establish an
106 alternative approach for targeting OMPs—the development of molecular plugs that block OMP
107 pores. Such plugs would allow for the manipulation of bacterial transport, providing a means of
108 either starving the bacterium by preventing the import of valuable nutrients or poisoning the
109 bacterium by preventing the export of toxins. Through real-time efflux assays, minimum
110 inhibitory concentration (MIC) experiments, we find that colE1-TR and colE1-T are able to
111 inhibit TolC-mediated efflux. We find that this plugging of TolC reduces the amount of
112 antibiotics required to inhibit the bacterial growth—indicating that this colicin E1 fragment
113 reduces the antibiotic resistance conferred by TolC.

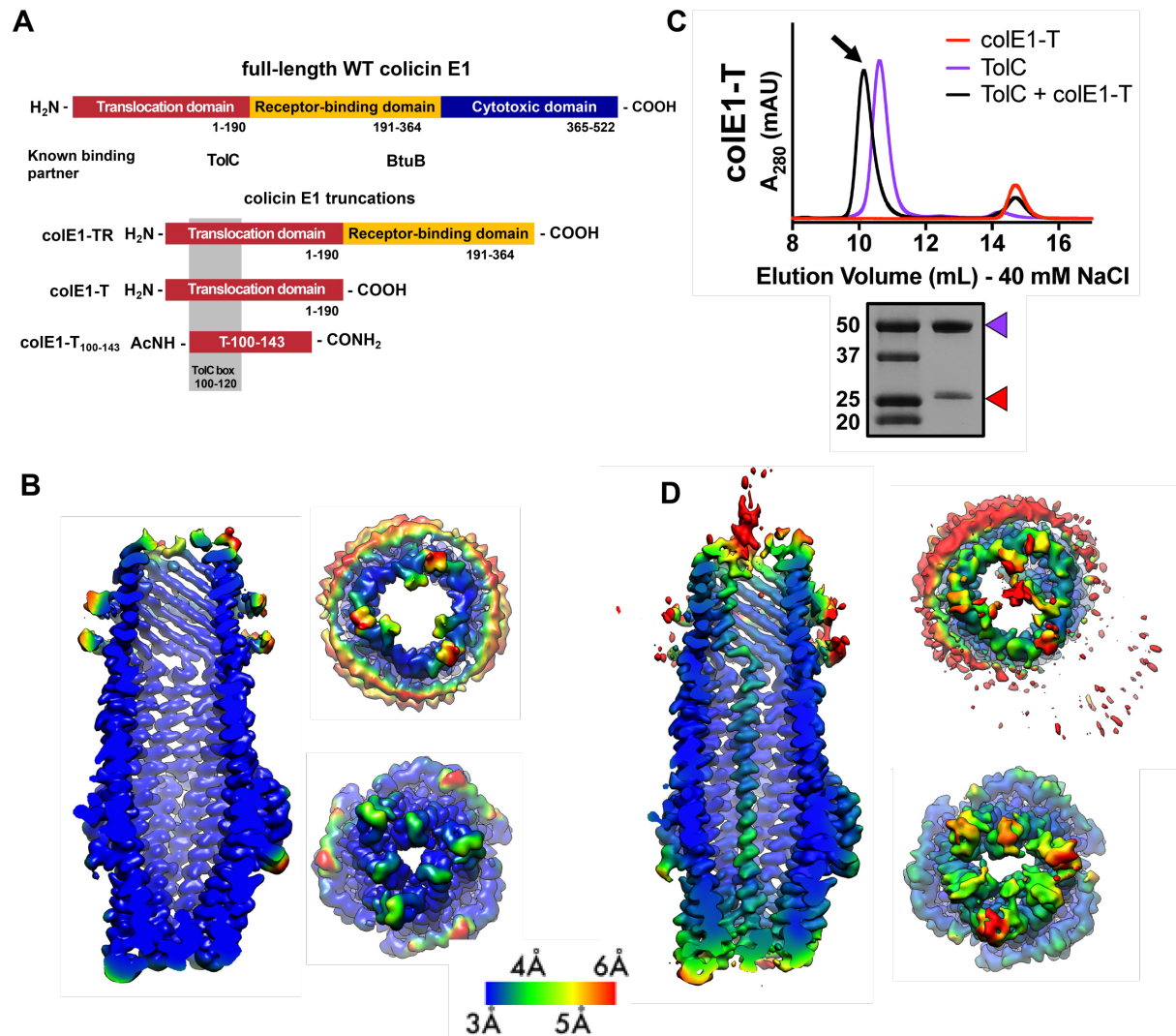


Figure 1. Cell-surface localization of colicin E1 fragments. (A) Architecture of full-length colicin E1 showing domains and their known binding partners. Three truncation constructs used in this study (B) CryoEM structure of TolC embedded in nanodiscs. Side, top, and bottom views are colored by local resolution, as computed in cryoSPARC from the final half-maps. The side view is cropped to display the particle interior. (C) SEC chromatogram of colE1-T (red line) and TolC (purple line). The arrow indicates the co-elution (black line) fractions that were analyzed by SDS-PAGE. On the SDS-PAGE gel (bottom), red arrows indicate the presence of the colicin E1 construct that has co-eluted with TolC. (D) The CryoEM structure of colE1-T bound to TolC and colored by local resolution as in (B).

115 **RESULTS**

116 **CryoEM structure of TolC embedded in nanodiscs**

117 To determine the structural details of colicin E1 binding to TolC, we solved the cryoEM
118 (cryogenic electron microscopy) structure of TolC embedded in nanodiscs with and without
119 added colE1-T (PDB 6WXH and 6WXI, respectively). We recently reported a high-yield TolC
120 preparation by refolding from inclusion bodies²⁸ and inserted refolded TolC into nanodiscs. The
121 cryoEM structure of refolded TolC alone (Figure 1B) is similar to the previously published
122 crystal structures of natively derived TolC alone²⁹ or in complex with hexammincobalt³⁰ but
123 with more splayed loops at the periplasmic opening (residues 165-175). There was local
124 variation in resolution within the model with lower resolution associated with the
125 extracellular/periplasmic ends and the nanodisc scaffold protein (Figure 1B). The lower residue
126 resolution at these apertures may indicate dynamics not captured in the x-ray crystal structures.

127 We next determined binding of colicin E1-T domain to capture the complex for structure
128 determination. Residues 1-190 (colE1-T) which span the translocation domain and are known to
129 bind to TolC (Figure 1A). We determined colE1-T:TolC binding *in vitro* via co-elution by size
130 exclusion chromatography (SEC) as previously described⁶. When colE1-T and TolC were
131 mixed, we observed a leftward shift in the TolC peak and a decrease in intensity associated with
132 the colE1-T peak indicating that a subset of the population has migrated with TolC (Figure 1C).
133 We analyzed the peak (Figure 1C arrow) using SDS-PAGE and found the presence of both
134 colE1-T and TolC. The unimodal shifted peak observed with colE1-T:TolC indicates that there is
135 a single species of fully bound TolC. When resolved by cryoEM, addition of colE1-T to TolC
136 breaks the three-fold channel symmetry and the additional protein is observed running all the
137 way through the TolC barrel as a single-pass, all- α -helical chain spanning more than 130 Å

138 (Figure 1D). The maps refined to nominal global resolutions of 2.84 Å and 3.09 Å for the TolC
139 and colE1-T:TolC, respectively (Table S1).

140 The colE1 T domain inserts into TolC with its amino terminus pointing inwards through
141 the periplasmic iris, and 2D class-averages show that the carboxy terminus of the helix continues
142 and projects out into the extracellular space (Figure 2A). 85 of the 190 colE1-T residues could be
143 modeled to this density (residues 46-131) (Figure 2B). No such regular protrusion was seen for
144 the glycine-rich colE1 amino-terminus, which we expect to be disordered in the periplasmic

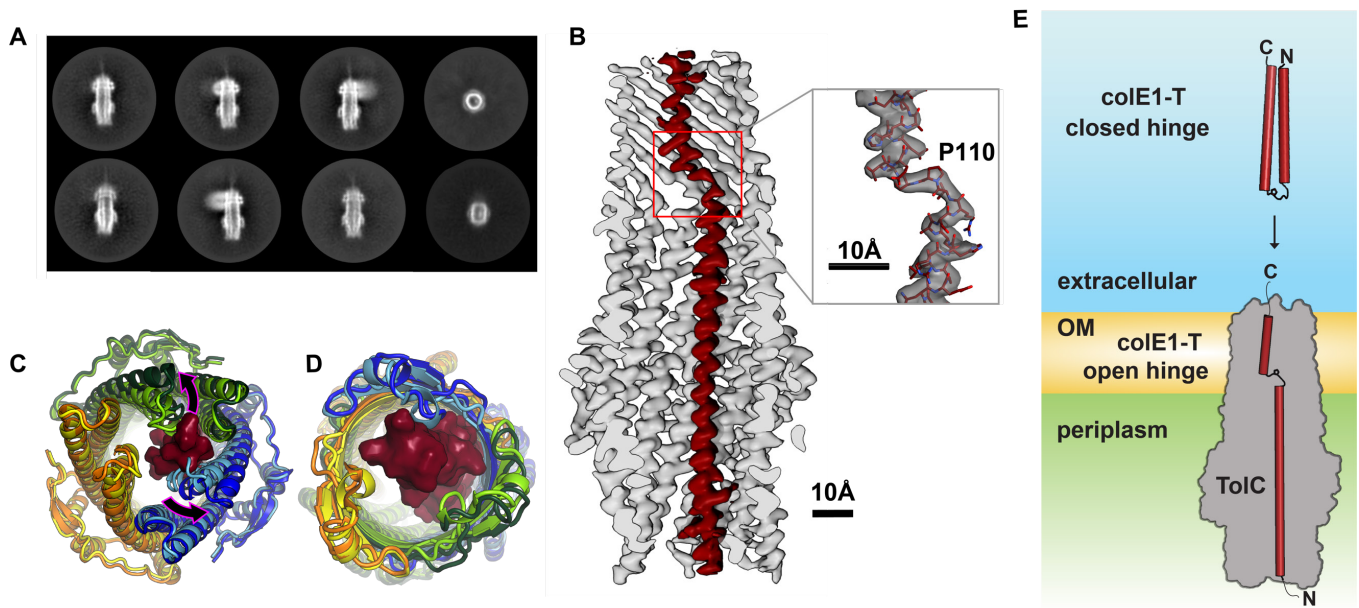


Figure 2. Colicin E1 binds to TolC as a single-pass kinked helix. (A) 2D class averages of colE1-T bound to TolC imbedded in nanodiscs (B) Cutaway view of the TolC interior (gray). ColE1-T (red) binds asymmetrically in an open-hinge conformation. The hinge region of colE1T including P110 shown in stick representation (inset). (C and D) The dilated terminal apertures. The apo cryoEM structure of TolC (subunits colored light blue, light green, and yellow) compared to holo cryoEM structure (subunits colored dark blue, dark green and orange). (C) Periplasmic aperture. (D) Extracellular aperture. (E) In the unbound state, colE1-T (red cylinders) exists as a closed hinge. When bound, colE1-T is in an open-hinge conformation through TolC with the N-terminus into the pore of TolC (grey). The homology model of colE1-T in its solution state was built using I-TASSER⁴ and is consistent with previous experiments⁶.

145 space^{22,26,31}. The colE1 chain binds TolC asymmetrically, primarily contacting only one of the
146 three TolC chains.

147 Compared to the unbound state, asymmetric colE1 binding dilates the periplasmic TolC
148 aperture (Figure 2C) and, to a lesser extent, the extracellular aperture (Figure 2D) so that they
149 can accommodate colE1 in the absence of any other proteins or motive force. Although the
150 terminal apertures dilate and are filled by the ligand and the TolC box forms specific interactions
151 with the TolC inner wall, the large internal volume of TolC is not fully occupied by colE1.

152 In solution, unbound colicin E1 is a two-helix hairpin as indicated by far UV circular
153 dichroism (CD)⁶. A homology model built using I-TASSER⁴ also predicts the closed hinge
154 conformation with proline 110 at the apex (Figure 2E top). However, our cryoEM reconstruction
155 of colicin E1 in complex with TolC shows that colE1-T hinges open at the TolC box to an
156 extended conformation upon binding to TolC (Figure 2B, and 2E bottom). The colE1-T helices
157 have a short kink in the middle around proline 110, precisely at the proposed turn location in the
158 hairpin model (Figure 2B inset). This area is also the center of the TolC box that has been known
159 to be critical for the colE1:TolC interaction^{22,24}.

160

161 **Colicin E1 makes residue-specific interactions with TolC**

162 TolC forms a large rigid conduit in the outer membrane and periplasm (Figure
163 3A) with a water filled lumen. The hydrophilic nature of the channel³² coupled with the
164 inflexibility of the outer-membrane-embedded barrel largely precludes the formation of any
165 hydrophobic interfaces that are typically the basis of protein-protein interfaces involving helical

166 peptides. Yet, we did observe specific polar contacts between colicin E1's TolC box and the
167 TolC barrel.

168 To obtain the most accurate atomic model for interpretation of atomic interactions
169 between peptides, we utilized map-restrained molecular dynamics in model refinement³³. The
170 refined model had improved chemical plausibility (for instance, MolProbity³⁴ score improved
171 from 1.25 to 0.50) and polar contact were more easily identified. Because this refinement

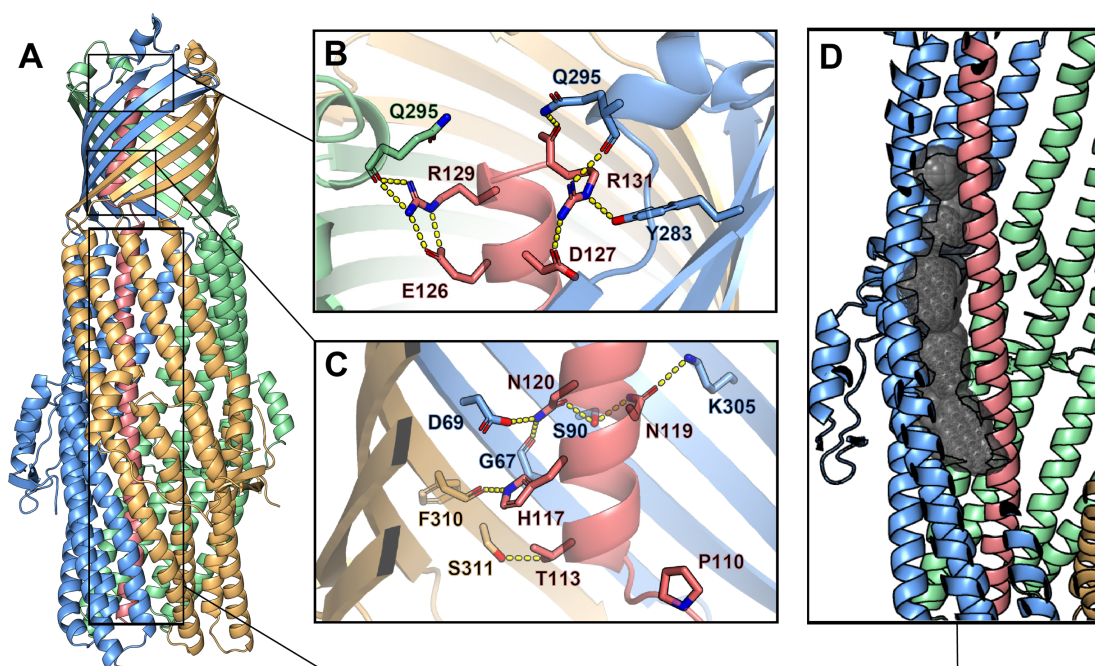


Figure 3. Inter-chain contacts between colE1T and TolC. (A) Molecular dynamics simulation refined structure of the colE1-T:TolC complex colored by chain (colE1-T: light red, TolC: light blue, light green, light gold) (B-C) Polar interaction network of colE1-T and TolC on the C-terminal side of the proline kink in the β -barrel region. (B) near the extracellular opening of TolC and (C) before the transition to the TolC periplasmic helical region. Residues involved in forming polar interactions and proline 110 are shown in sticks. (D) ColE1-T spanning the TolC helical barrel does not make full contact with the side of the TolC barrel. The cavity (black spheres) between colicin (light red) and one chain of TolC (light blue) was detected using GHECOM¹⁻³

172 improved the concordance between the map and model, we conclude that the use of cryoEM
173 density as a restraint was successful in preventing overfitting. Specifically, the EMRinger³⁵ score
174 improved from 2.77 to 3.81 and the map-model FSC=0.5 improved from 3.44Å to 3.37Å.

175 The atomic model showed significant polar interactions form between colicin E1 and
176 TolC at the apertures and around the TolC box. The acidic patch of colicin E1 near the
177 extracellular aperture contains two arginine residues (R129 and R131) that form hydrogen bond
178 networks with one TolC chain each (Figure 3B). In addition, colicin E1 residues T113, A116,
179 N119, N120 (all part of the TolC box) establish polar interactions with TolC residues G67, D69,
180 S90 and K305 on one TolC chain (Figure 3C, light red and light blue) while colicin H117
181 interacts with TolC F310 on a neighboring TolC chain (Figure 3C, light red and light gold). By
182 contrast with the β -barrel of TolC, in the interior of periplasmic helical barrel of TolC, colicin E1
183 does not make full contact with the α -helical barrel interior and there is a gap between the two
184 proteins (Figure 3D). This is in agreement with previous studies that showed a colicin truncation
185 (residues 1-100) that ends just before the beginning of the TolC box does not bind to TolC²² or
186 prevent cytotoxicity of full-length colicin in cells²⁴.

187 Moreover, this structure is consistent with reports that mutations at TolC sites G43 or
188 S257 abrogate colE1 activity³⁶ as these residues are contact sites between TolC and colE1
189 (Figure S1). Conversely, the absence of any effect of mutating colicin R103 and R108²⁴, is
190 consistent with interaction those residues have with the barrel solvent rather than TolC. The
191 newly solved structure, in combination with previous work^{22,24}, indicates the specificity of
192 colicin E1 binding to TolC is encoded in the portion that binds to TolC β -barrel.

193 **Membrane localization of colE1 truncations**

194 Since we find the colE1 T domain binds to TolC, we investigated if colicin E1 fragments
195 bind to the native TolC in *E. coli* cells. Though ColE1 C domain activity—depolarizing the inner
196 membrane—requires the C domain to pass through the outer membrane³⁷, it remains unclear if
197 the colE1-TR domains translocate as well. We first determined *in vitro* binding of colE1-TR,

198 which includes residues 1-364 (colE1-TR) (Figure 1A) which contains the N-terminal portion
199 that binds to TolC and the C-terminal portion that binds to BtuB. ColE1-TR aggregates at the salt
200 concentration (40 mM) used for the co-elution experiment used for colE1-T so we increased the
201 NaCl concentration to 200 mM. ColE1-T still binds to TolC at 250 mM NaCl although to a much
202 lesser degree (Figure S2). Unlike colE1-T (Figure 1C), colE1-TR shows a bimodal distribution
203 indicative of a mixed population of bound and unbound TolC (Figure 4A). Using an extracellular
204 protease digestion assay, we assessed whether colE1-T and colE1-TR translocate into the cell or
205 localize on the cell surface. ColE1 fragments were incubated with cells, washed, and treated with
206 or without trypsin to digest any extracellularly bound protein to cells. When probing for the C-
207 terminal epitope by immunoblotting, there was no detectible colE1-T binding (Figure 4B, left),
208 though there was detectible binding of ColE1-TR (Figure 4B, right). Moreover, we found that if
209 colE1-TR is incubated with cells and subsequently treated with increasing trypsin concentrations,
210 the colE1-TR band disappeared, indicating that the colicin E1 fragment was localized to the
211 outer membrane surface (Figure 4B, right). The colE1-TR band of the intact cells may be slightly
212 less intense than the colE1 band for lysed cells due to some aggregation and precipitation of the
213 intact cell and proteins bound to it when boiling the whole cells for loading the SDS-PAGE. The
214 periplasmic control SurA was not degraded at any trypsin concentration unless the cells were
215 lysed before trypsin digestion³⁸.

216 Since the proteolysis experiments are not sensitive enough to detect if only a few
 217 molecules have entered the cell, we further probed the interaction between the cell membrane
 218 and surface-localized colE1-TR with single-molecule fluorescence microscopy using the
 219 fluorescent dye Cy3. This method is able to detect single molecules on the cell surface as well as
 220 those within the cell indicative of those molecules having crossed the outer membrane^{39,40}. When
 221 colE1-TR-Cy3 was added to the extracellular environment of WT BW25113 *E. coli* (containing
 222 TolC), distinct puncta (Figure 4C, left) formed on 94% of the cells ($n = 111$) (Figure 4D). In a
 223 $\Delta tolC$ strain, puncta were observed on only 18% of cells ($n = 99$) (Figure 4C, right; Figure 4D).
 224 As a $\Delta btuB$ control strain, we used BL21 (DE3) which is known to have a premature stop codon
 225 at *btuB* residue 58⁴¹. Puncta were observed on only 3% of cells lacking BtuB ($n = 105$) (Figure
 226 4D and S3A). In WT and $\Delta tolC$ cells that featured puncta, colE1-TR formed puncta consistent

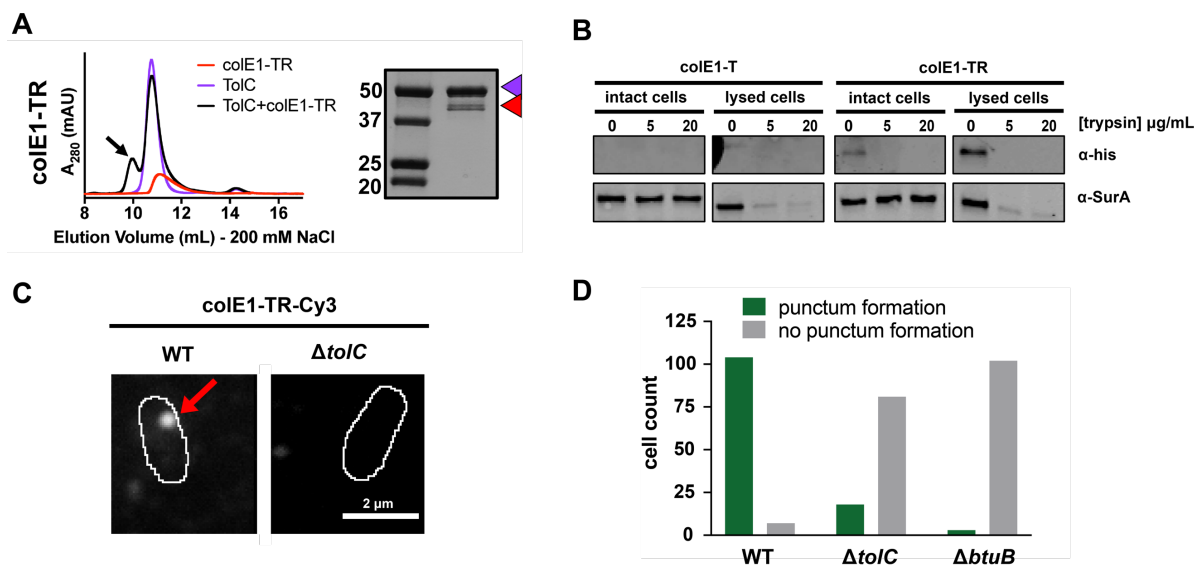


Figure 4. Colicin E1-TR localizes on the outside of the cell. (A) SEC chromatogram of colE1-TR (red line) and TolC (purple line). The arrow indicates the co-elution (black line) fractions that were analyzed by SDS-PAGE. On the SDS-PAGE gels (right), red arrow indicates the presence of colicin E1 construct that has co-eluted with TolC (purple arrow). (B) Extracellular protease digestion assay with two colicin E1 truncation constructs, each labeled with a C-terminal His-Tag. Periplasmic SurA was used as a membrane integrity control. (C) Fluorescence image of colE1-TR-Cy3 overlaid on outlines of living *E. coli* cells for WT and $\Delta tolC$. Red arrow points to a punctum. (D) Cell counts where colE1-TR-Cy3 punctum formation was observed for WT, $\Delta tolC$, and $\Delta btuB$.

227 with ~20 molecules. The observed size and number of molecules are in agreement with previous
228 studies of BtuB puncta^{42,43}. To rule out punctum formation as an artifact of Cy3 conjugation, we
229 found colE1-TR-GFP displayed the same cluster formation as colE1-TR-Cy3 (Figure S3B). No
230 other single protein binding events were detected aside from the puncta on either WT or $\Delta tolC$
231 cells.

232 Fluorescently labeled pyocins, the colicin analog in *Pseudomonas*, have previously been
233 used to detect translocation across the outer membrane of *Pseudomonas aeruginosa*⁴⁴. Here we
234 use an analogous experiment with fluorescently labeled colE1 to determine cellular localization
235 in *E. coli*. In time courses, bound colE1-TR puncta remained immobile for > 5 minutes (Movie
236 S1). This is consistent with continued association of colE1-TR with membrane-embedded BtuB,
237 which has limited mobility⁴⁵. This result indicates that colE1-TR does not fully translocate⁴⁴,
238 because if colE1-TR entered the periplasmic space it would freely diffuse on these timescales.

239 Colicin constructs lacking the R domain (colE1-T-Cy3) showed no detectable binding
240 either to WT or $\Delta tolC$ cells (Figure S3C), indicating that the TolC-colE1-T interaction is much
241 weaker than the BtuB-colE1-TR interaction.

242 Because we only see one punctum per cell, we anticipate that some BtuB and TolC
243 remain unbound because of the geometric constraints of punctum formation. Though BtuB and
244 TolC need to be in close proximity for colE1 binding to occur, when BtuB clusters together in
245 groups of 12 or more, it may exclude TolC. These cluster geometries would therefore lower the
246 number of full binding sites available for the T and R domains of colicin E1.

247

248 **ColE1-TR inhibits efflux and makes *E. coli* more susceptible to antibiotics**

249 Since the colicin truncations are stalled on their respective OMP receptors, we

250 investigated if this stalling could disrupt native TolC efflux. Real-time efflux inhibition by

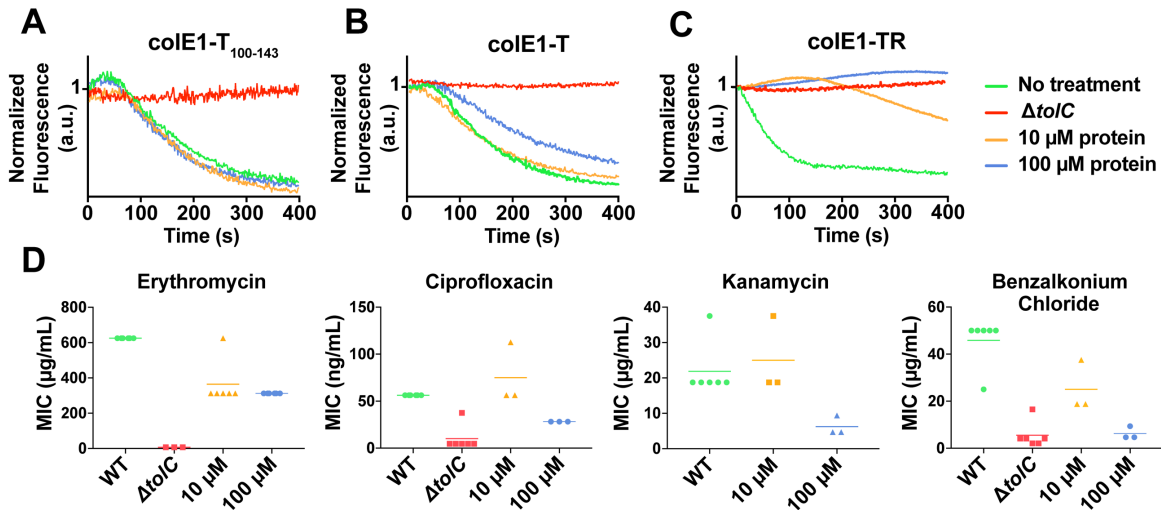


Figure 5. Colicin E1 fragments inhibit efflux and potentiate antibiotics.

(A-C) Effect of colicin E1 fragments on efflux: WT with no protein (green), $\Delta tolC$ (red), WT + 10 μM (orange), WT + 100 μM protein (blue). (A) colE1-T₁₀₀₋₁₄₃, (B) colE1-T, (C) colE1-TR. (D) Antibiotic susceptibilities in the absence (green) and presence of colE1-TR added to WT at 10 μM (orange) and 100 μM (blue). MICs for $\Delta tolC$ (red) are included as a reference. Data are biological replicates reported as the mean and individual data points.

251 colicin E1 fragments was assessed using a live-cell assay with N-(2-naphthyl)-1-naphthylamine
252 (NNN)-dye, which is effluxed by the acridine efflux pump and fluoresces when it is localized
253 inside the cell⁴⁶. NNN efflux can be turned off by the protonophore CCCP, which neutralizes the
254 proton motive force and allows NNN to accumulate within the cell. Active efflux can then be
255 monitored by the fluorescence decay once proton motive force is reenergized by glucose
256 addition⁴⁶⁻⁵⁰.

257 We assessed the ability of colicin E1 truncations to plug TolC by monitoring real-time
258 NNN efflux. Cells exposed to colE1-T₁₀₀₋₁₄₃ did not show lower real-time efflux than untreated

259 cells (Figure 5A). This observation is notable in light of the fact that, in previous conductance
260 studies, similar peptides were shown to bind TolC^{6,24} and to occlude the channel^{6,23}.

261 Cells exposed to colE1-T showed less decay in final fluorescence than untreated cells,
262 indicating that colE1-T partially inhibits efflux (Figure 5B). Finally, exposure to colE1-TR
263 produced no decrease in fluorescence, showing full inhibition of efflux (Figure 5C).

264 Because colE1-TR completely inhibits NNN efflux, we evaluated the capacity of colE1-
265 TR to potentiate antibiotics representing four different classes that are known TolC substrates:
266 kanamycin, ciprofloxacin, erythromycin, and benzalkonium chloride (from aminoglycosides,
267 fluoroquinolones, macrolides, and quaternary ammonium compounds, respectively). An effective
268 TolC plug will reduce the concentration required to inhibit growth as antibiotics remain trapped
269 within the cell. WT *E. coli* cells that were exposed to 100 μ M colE1-TR with each of these
270 antibiotics showed significantly lower minimum inhibitory concentrations (MICs), the lowest
271 concentration of antibiotic that inhibits visible growth, than cells exposed to the antibiotics alone
272 (Fig. 5D): exposure to 100 μ M colE1-TR made WT *E. coli* ~2 to 7-fold more susceptible to these
273 antibiotics (Table S2). Engagement of TolA by the N-terminal TolA box of colicin E9 has
274 previously been shown to cause outer membrane defects⁵¹ which would lead to enhanced
275 antibiotic susceptibility. To rule out outer membrane-mediated defects caused by the TolA box in
276 colE1, we created a truncation of colE1-TR (colE1-TR $_{\Delta 1-40}$) lacking the N-terminal 40 residues
277 including the TolA box. The MIC of colE1-TR and colE1-TR $_{\Delta 1-40}$ are identical (Figure S4)
278 indicating that colE1-TR engagement of TolA does not contribute to the observed antibiotic
279 susceptibility.

280 Discussion

281 There are two conflicting models of colE1 translocation: 1) the total thread model in
282 which the entire colicin unfolds and threads through TolC^{24,52} and 2) the pillar model, in which
283 colicin E1 inserts into TolC as a helical hairpin, facilitating LPS-mediated self-translocation of
284 the colicin cytotoxic domain⁶. Our data support aspects of both models. The belief in a closed
285 hinge conformation of bound colE1 prompted two arguments against the total thread mechanism:
286 1) the colE1-T closed hinge conformation is too wide to fit through TolC and 2) both ends would
287 face the extracellular milieu^{6,52}. The unanticipated colE1-T hinge opening in the bound state
288 resolves these objections: colicin threads into the TolC barrel with the amino terminus pointing
289 into the periplasm, as the total thread model hypothesized. However, our trypsin digests and
290 single-molecule fluorescence images show colE1-TR stalls at the outer membrane. Though we
291 cannot exclude the possibility that full length protein translocation depends on the C domain, we
292 observe—as hypothesized by the pillar model—that colicin sits inside TolC but does not
293 translocate. However, the architecture of the complex differs from that hypothesized by the pillar
294 model. These results are in agreement with early studies of pore-forming colicins in which
295 trypsin added to the extracellular environment can reverse colicin activity. Digestibility by
296 trypsin, as well as the ability of colE1-T/TolC to reconstitute a monodisperse stable complex *in*
297 *vitro* are consistent with the colicin remain in contact with its outer membrane receptors while
298 the cytotoxic domain depolarizes the inner membrane.

299 In addition to demonstrating a colicin insertion mechanism, our observations form the
300 basis of a means to manipulate bacterial import and efflux. Though colicin E1 confers some level
301 of antibiotic potentiation, the relatively high concentration of colE1-TR needed to inhibit efflux
302 may be explained by a combination of the geometric constraints of creating large clusters of

303 BtuB and TolC, low colE1-T-TolC affinity⁵³, and residually unblocked pore, even in the bound
304 state. Because of their limited potency, our colE1-T and colE1-TR fragments are not likely to be
305 practical in direct applications of antibiotic potentiation. However, our proof-of-concept findings
306 offer a potential roadmap for further development. A more potent TolC binder would not need
307 the R domain anchor for affinity. Such a binder could be designed using the atomic details of the
308 colE1-T-TolC structure as a basis. Moreover, this scaffold can be used for efflux pump inhibitors
309 for at least five other bacterial organisms. Each of these organisms has a structurally
310 characterized outer membrane efflux pump that is homologous and structurally similar to TolC⁵⁴.

311 More broadly, there are at least nine known outer membrane protein receptors for
312 bacteriocins. These outer membrane proteins have a variety of functions including adhesion, iron
313 transport, and general import^{12,55}. Using this same strategy with fragments derived from other
314 bacteriocins may additionally allow for controlled inhibition of other bacterial functions.

315 **Acknowledgments** We gratefully acknowledge Daniel Montezano, Pinakin Sukthankar, Rik
316 Dhar, Dwight Deay, Scott Lovell, Matthias Wolf, Alexander Little, Heather Shinogle, and Sarah
317 Noga for discussions and feedback, Mark Richter for the use of his fluorometer, Rajeev Misra
318 for the pTrc vector containing the TolC gene, Vasileios Petrou for guidance on nanodiscs,
319 Chamani Perera for peptide synthesis, Karen Marom for editorial guidance. We thank the Office
320 of Advanced Research computing (OARC) at Rutgers for high-performance computing
321 resources. Funding: NIH award R21-GM128022 to JSB, NIGMS awards DP2GM128201,
322 P20GM113117, P20GM103638 and the Gordon and Betty Moore Inventor Fellowship to JSGS,
323 and NIGMS awards P20 GM103418 and 2K12GM063651 to SJB.

324 **Author contributions** Conceptualization: SJB, JSGS; Methodology: SJB, JTK, JSGS, JSB;
325 Writing: SJB, JSGS, JSB, JTK; Editing: SJB, JSGS, JSB, JTK; Investigation: SJB, JJS, ALC,
326 API, VKW, EF, DAC, and JTK.

327 **Competing interests** The authors declare no competing interests.

328
329

330

References

- 331 1. Kawabata, T. Detection of multiscale pockets on protein surfaces using mathematical
332 morphology. *Proteins* **78**, 1195-211 (2010).
- 333 2. Kawabata, T. Detection of cave pockets in large molecules: Spaces into which internal
334 probes can enter, but external probes from outside cannot. *Biophys Physicobiol* **16**, 391-
335 406 (2019).
- 336 3. Kawabata, T. & Go, N. Detection of pockets on protein surfaces using small and large
337 probe spheres to find putative ligand binding sites. *Proteins* **68**, 516-29 (2007).
- 338 4. Yang, J. et al. The I-TASSER Suite: protein structure and function prediction. *Nat*
339 *Methods* **12**, 7-8 (2015).
- 340 5. Alexander, C. & Rietschel, E.T. Invited review: Bacterial lipopolysaccharides and innate
341 immunity. *Journal of Endotoxin Research* **7**, 167-202 (2001).
- 342 6. Zakharov, S.D., Wang, X.S. & Cramer, W.A. The Colicin E1 TolC-Binding Conformer:
343 Pillar or Pore Function of TolC in Colicin Import? *Biochemistry* **55**, 5084-5094 (2016).
- 344 7. Kamio, Y. & Nikaido, H. Outer membrane of *Salmonella typhimurium*: accessibility of
345 phospholipid head groups to phospholipase c and cyanogen bromide activated dextran in
346 the external medium. *Biochemistry* **15**, 2561-70 (1976).
- 347 8. Freeman, J.T.C. & Wimley, W.C. TMBB-DB: a transmembrane β -barrel proteome
348 database. *Bioinformatics* **28**, 2425-2430 (2012).
- 349 9. Cramer, W.A., Sharma, O. & Zakharov, S.D. On mechanisms of colicin import: the outer
350 membrane quandary. *Biochem J* **475**, 3903-3915 (2018).
- 351 10. Buchanan, S.K. et al. Structure of colicin I receptor bound to the R-domain of colicin Ia:
352 implications for protein import. *EMBO J* **26**, 2594-604 (2007).
- 353 11. Kurisu, G. et al. The structure of BtuB with bound colicin E3 R-domain implies a
354 translocon. *Nat Struct Biol* **10**, 948-54 (2003).
- 355 12. Cascales, E. et al. Colicin Biology. *Microbiology and Molecular Biology Reviews* **71**,
356 158-229 (2007).
- 357 13. Housden, N.G. et al. Directed epitope delivery across the *Escherichia coli* outer
358 membrane through the porin OmpF. *Proc Natl Acad Sci U S A* **107**, 21412-7 (2010).
- 359 14. Sharma, O. et al. Structure of the complex of the colicin E2 R-domain and its BtuB
360 receptor. The outer membrane colicin translocon. *J Biol Chem* **282**, 23163-70 (2007).
- 361 15. Benedetti, H. et al. Individual domains of colicins confer specificity in colicin uptake, in
362 pore-properties and in immunity requirement. *J Mol Biol* **217**, 429-39 (1991).
- 363 16. Benedetti, H. et al. Comparison of the Uptake Systems for the Entry of Various BtuB
364 Group Colicins into *Escherichia coli*. *Microbiology* **135**, 3413-3420 (1989).
- 365 17. Elkins, P., Bunker, A., Cramer, W.A. & Stauffacher, C.V. A mechanism for toxin
366 insertion into membranes is suggested by the crystal structure of the channel-forming
367 domain of colicin E1. *Structure* **5**, 443-58 (1997).
- 368 18. Plate, C.A. & Luria, S.E. Stages in colicin K action, as revealed by the action of trypsin.
369 *Proc Natl Acad Sci U S A* **69**, 2030-4 (1972).
- 370 19. Dankert, J., Hammond, S.M. & Cramer, W.A. Reversal by trypsin of the inhibition of
371 active transport by colicin E1. *J Bacteriol* **143**, 594-602 (1980).
- 372 20. Dankert, J.R., Uratani, Y., Grabau, C., Cramer, W.A. & Hermodson, M. On a domain
373 structure of colicin E1. A COOH-terminal peptide fragment active in membrane
374 depolarization. *J Biol Chem* **257**, 3857-63 (1982).

- 375 21. Benedetti, H., Lloubes, R., Lazdunski, C. & Letellier, L. Colicin A unfolds during its
376 translocation in Escherichia coli cells and spans the whole cell envelope when its pore
377 has formed. *EMBO J* **11**, 441-7 (1992).
- 378 22. Zakharov, S.D., Wang, X.S. & Cramer, W.A. The Colicin E1 TolC-Binding Conformer:
379 Pillar or Pore Function of TolC in Colicin Import? *Biochemistry* **55**, 5084-94 (2016).
- 380 23. Zakharov, S.D. et al. Colicin occlusion of OmpF and TolC channels: outer membrane
381 translocons for colicin import. *Biophys J* **87**, 3901-11 (2004).
- 382 24. Jakes, K.S. The Colicin E1 TolC Box: Identification of a Domain Required for Colicin
383 E1 Cytotoxicity and TolC Binding. *J Bacteriol* **199**(2017).
- 384 25. Wiener, M., Freymann, D., Ghosh, P. & Stroud, R.M. Crystal structure of colicin Ia.
385 *Nature* **385**, 461-4 (1997).
- 386 26. Housden, N.G. et al. Intrinsically disordered protein threads through the bacterial outer-
387 membrane porin OmpF. *Science* **340**, 1570-4 (2013).
- 388 27. Storek, K.M. et al. Monoclonal antibody targeting the beta-barrel assembly machine of
389 Escherichia coli is bactericidal. *Proc Natl Acad Sci U S A* **115**, 3692-3697 (2018).
- 390 28. Budiardjo, S.J. et al. High-Yield Preparation of Outer Membrane Protein Efflux Pumps
391 by in Vitro Refolding is Concentration Dependent. *J Membr Biol* **254**, 41-50 (2021).
- 392 29. Koronakis, V., Sharff, A., Koronakis, E., Luisi, B. & Hughes, C. Crystal structure of the
393 bacterial membrane protein TolC central to multidrug efflux and protein export. *Nature*
394 **405**, 914-9 (2000).
- 395 30. Higgins, M.K. et al. Structure of the ligand-blocked periplasmic entrance of the bacterial
396 multidrug efflux protein TolC. *J Mol Biol* **342**, 697-702 (2004).
- 397 31. Housden, N.G. et al. Directional Porin Binding of Intrinsically Disordered Protein
398 Sequences Promotes Colicin Epitope Display in the Bacterial Periplasm. *Biochemistry*
399 **57**, 4374-4381 (2018).
- 400 32. Dhar, R., Feehan, R. & Slusky, J.S.G. Membrane Barrels Are Taller, Fatter, Inside-Out
401 Soluble Barrels. *J Phys Chem B* **125**, 3622-3628 (2021).
- 402 33. Wu, X., Subramaniam, S., Case, D.A., Wu, K.W. & Brooks, B.R. Targeted
403 conformational search with map-restrained self-guided Langevin dynamics: application
404 to flexible fitting into electron microscopic density maps. *J Struct Biol* **183**, 429-440
405 (2013).
- 406 34. Williams, C.J. et al. MolProbity: More and better reference data for improved all-atom
407 structure validation. *Protein Sci* **27**, 293-315 (2018).
- 408 35. Barad, B.A. et al. EMRinger: side chain-directed model and map validation for 3D cryo-
409 electron microscopy. *Nat Methods* **12**, 943-6 (2015).
- 410 36. Masi, M., Vuong, P., Humbard, M., Malone, K. & Misra, R. Initial steps of colicin E1
411 import across the outer membrane of Escherichia coli. *J Bacteriol* **189**, 2667-76 (2007).
- 412 37. Brunden, K.R., Uratani, Y. & Cramer, W.A. Dependence of the conformation of a colicin
413 E1 channel-forming peptide on acidic pH and solvent polarity. *J Biol Chem* **259**, 7682-7
414 (1984).
- 415 38. Besingi, R.N. & Clark, P.L. Extracellular protease digestion to evaluate membrane
416 protein cell surface localization. *Nat Protoc* **10**, 2074-80 (2015).
- 417 39. Tuson, H.H. & Biteen, J.S. Unveiling the inner workings of live bacteria using super-
418 resolution microscopy. *Anal Chem* **87**, 42-63 (2015).

- 419 40. Al-Husini, N. et al. BR-Bodies Provide Selectively Permeable Condensates that
420 Stimulate mRNA Decay and Prevent Release of Decay Intermediates. *Mol Cell* **78**, 670-
421 682 e8 (2020).
- 422 41. Studier, F.W., Daegelen, P., Lenski, R.E., Maslov, S. & Kim, J.F. Understanding the
423 differences between genome sequences of Escherichia coli B strains REL606 and
424 BL21(DE3) and comparison of the E. coli B and K-12 genomes. *J Mol Biol* **394**, 653-80
425 (2009).
- 426 42. Rassam, P. et al. Supramolecular assemblies underpin turnover of outer membrane
427 proteins in bacteria. *Nature* **523**, 333-6 (2015).
- 428 43. Chavent, M. et al. How nanoscale protein interactions determine the mesoscale dynamic
429 organisation of bacterial outer membrane proteins. *Nat Commun* **9**, 2846 (2018).
- 430 44. White, P. et al. Exploitation of an iron transporter for bacterial protein antibiotic import.
431 *Proc Natl Acad Sci U S A* **114**, 12051-12056 (2017).
- 432 45. Kleanthous, C., Rassam, P. & Baumann, C.G. Protein-protein interactions and the
433 spatiotemporal dynamics of bacterial outer membrane proteins. *Curr Opin Struct Biol* **35**,
434 109-15 (2015).
- 435 46. Bohnert, J.A., Schuster, S., Szymaniak-Vits, M. & Kern, W.V. Determination of real-
436 time efflux phenotypes in Escherichia coli AcrB binding pocket phenylalanine mutants
437 using a 1,2'-dinaphthylamine efflux assay. *PLoS One* **6**, e21196 (2011).
- 438 47. Bohnert, J.A., Karamian, B. & Nikaido, H. Optimized Nile Red efflux assay of AcrAB-
439 TolC multidrug efflux system shows competition between substrates. *Antimicrob Agents*
440 *Chemother* **54**, 3770-5 (2010).
- 441 48. Seeger, M.A. et al. Engineered disulfide bonds support the functional rotation mechanism
442 of multidrug efflux pump AcrB. *Nat Struct Mol Biol* **15**, 199-205 (2008).
- 443 49. Iyer, R., Ferrari, A., Rijnbrand, R. & Erwin, A.L. A fluorescent microplate assay
444 quantifies bacterial efflux and demonstrates two distinct compound binding sites in AcrB.
445 *Antimicrob Agents Chemother* **59**, 2388-97 (2015).
- 446 50. Misra, R., Morrison, K.D., Cho, H.J. & Khuu, T. Importance of Real-Time Assays To
447 Distinguish Multidrug Efflux Pump-Inhibiting and Outer Membrane-Destabilizing
448 Activities in Escherichia coli. *J Bacteriol* **197**, 2479-88 (2015).
- 449 51. Rassam, P. et al. Intermembrane crosstalk drives inner-membrane protein organization in
450 Escherichia coli. *Nat Commun* **9**, 1082 (2018).
- 451 52. Cramer, W.A., Sharma, O. & Zakharov, S.D. On mechanisms of colicin import: the outer
452 membrane quandary. *Biochemical Journal* **475**, 3903-3915 (2018).
- 453 53. Taylor, R., Burgner, J.W., Clifton, J. & Cramer, W.A. Purification and characterization of
454 monomeric Escherichia coli vitamin B12 receptor with high affinity for colicin E3. *J Biol*
455 *Chem* **273**, 31113-8 (1998).
- 456 54. Franklin, M.W. et al. Efflux Pumps Represent Possible Evolutionary Convergence onto
457 the beta-Barrel Fold. *Structure* **26**, 1266-1274.e2 (2018).
- 458 55. Kleanthous, C. Swimming against the tide: progress and challenges in our understanding
459 of colicin translocation. *Nat Rev Microbiol* **8**, 843-8 (2010).
- 460 56. Hagn, F., Nasr, M.L. & Wagner, G. Assembly of phospholipid nanodiscs of controlled
461 size for structural studies of membrane proteins by NMR. *Nat Protoc* **13**, 79-98 (2018).
- 462 57. Wiegand, I., Hilpert, K. & Hancock, R.E. Agar and broth dilution methods to determine
463 the minimal inhibitory concentration (MIC) of antimicrobial substances. *Nat Protoc* **3**,
464 163-75 (2008).

- 465 58. Daury, L. et al. Tripartite assembly of RND multidrug efflux pumps. *Nat Commun* **7**,
466 10731 (2016).
467 59. Weis, F. & Hagen, W.J.H. Combining high throughput and high quality for cryo-electron
468 microscopy data collection. *Acta Crystallogr D Struct Biol* **76**, 724-728 (2020).
469 60. Mastronarde, D.N. Advanced Data Acquisition From Electron Microscopes With
470 SerialEM. *Microscopy and Microanalysis* **24**, 864-865 (2018).
471 61. Rice, W.J. et al. Routine determination of ice thickness for cryo-EM grids. *J Struct Biol*
472 **204**, 38-44 (2018).
473 62. Budiardjo, S.J. et al. High yield preparation of outer-membrane protein efflux pumps by
474 in vitro refolding is concentration dependent. *bioRxiv*,
475 2020.09.14.296756 (2020).
476 63. Punjani, A., Rubinstein, J.L., Fleet, D.J. & Brubaker, M.A. cryoSPARC: algorithms for
477 rapid unsupervised cryo-EM structure determination. *Nat Methods* **14**, 290-296 (2017).
478 64. Zivanov, J. et al. New tools for automated high-resolution cryo-EM structure
479 determination in RELION-3. *Elife* **7**(2018).
480 65. Rohou, A. & Grigorieff, N. CTFFIND4: Fast and accurate defocus estimation from
481 electron micrographs. *J Struct Biol* **192**, 216-21 (2015).
482 66. Wagner, T. et al. SPHIRE-crYOLO is a fast and accurate fully automated particle picker
483 for cryo-EM. *Commun Biol* **2**, 218 (2019).
484 67. Cardone, G., Heymann, J.B. & Steven, A.C. One number does not fit all: mapping local
485 variations in resolution in cryo-EM reconstructions. *J Struct Biol* **184**, 226-36 (2013).
486 68. Afonine, P.V. et al. Real-space refinement in PHENIX for cryo-EM and crystallography.
487 *Acta Crystallogr D Struct Biol* **74**, 531-544 (2018).
488 69. Croll, T.I. ISOLDE: a physically realistic environment for model building into low-
489 resolution electron-density maps. *Acta Crystallogr D Struct Biol* **74**, 519-530 (2018).
490 70. Emsley, P., Lohkamp, B., Scott, W.G. & Cowtan, K. Features and development of Coot.
491 *Acta Crystallogr D Biol Crystallogr* **66**, 486-501 (2010).
492 71. Maier, J.A. et al. ff14SB: Improving the Accuracy of Protein Side Chain and Backbone
493 Parameters from ff99SB. *J Chem Theory Comput* **11**, 3696-713 (2015).
494 72. Nguyen, H., Roe, D.R. & Simmerling, C. Improved Generalized Born Solvent Model
495 Parameters for Protein Simulations. *J Chem Theory Comput* **9**, 2020-2034 (2013).
496 73. Goddard, T.D. et al. UCSF ChimeraX: Meeting modern challenges in visualization and
497 analysis. *Protein Sci* **27**, 14-25 (2018).
498

499 **RESOURCE AVAILABILITY**

500 **KEY RESOURCES TABLE**

REAGENT or RESOURCE	SOURCE	IDENTIFIER
Antibodies		
THE HisTag mAb Mouse	GenScript	Cat#A00186-100; RRID:19J001957
anti-SurA Rabbit polyclonal	Cusabio	Cat#CSB- PA359693HA01ENV; RRID:E0109A
IRDye 800CW goat anti-mouse IgG secondary	LI-COR	Cat#925-32210; RRID:C81106-01

IRDye 800CW Donkey anti-Rabbit	LI-COR	Cat#925-32213; RRID:C80829-10
Bacterial and Virus Strains		
BW25113	Coli Genetic Stock Center	Cat#7636
JW5503-1	Coli Genetic Stock Center	Cat#11430
BL21(DE3)	Coli Genetic Stock Center	Cat#12504
Chemicals, Peptides, and Recombinant Proteins		
ToIC	This paper	N/A
ColE1-T	This paper	N/A
ColE1-TR	This paper	N/A
ColE1-T100-143	This paper	N/A
Deposited Data		
ToIC alone map	This paper	EMDB-21960 PDB 6WXI
ToIC-colE1-T complex map	This paper	EMDB-21959 PDB 6WXH
Recombinant DNA		
pTrc99a-NoSS-ToIC	This paper	Addgene
pET303-colE1-T	This paper	Addgene
pET303-colE1-TR	This paper	Addgene
MSP1D1	Addgene	Cat#20061
Software and Algorithms		
cryoSPARC 2 v2.12	Punjani, Rubinstein et al. 2017	https://cryosparc.com/
phenix v1.14-3260	Afonine, Poon et al. 2018	https://www.phenix-online.org/
serialEM v3.7	Mastrorade 2018	https://bio3d.colorado.edu/SerialEM/
coot v0.8.9.2-re 7766	Emsley, Lohkamp et al. 2010	https://www2.mrc-lmb.cam.ac.uk/personal/pemsley/coot/
ISOLDE v1.0b4.dev1	Croll 2018	https://isolde.cimr.cam.ac.uk/static/isolde/doc/tools/ISOLDE.html
UCSF ChimeraX	Goddard, Huang et al. 2018	https://www.cgl.ucsf.edu/chimerax/
PyMOL	Schrödinger, LLC	https://pymol.org/2/

501
502
503
504
505
506

RESOURCE AVAILABILITY

Lead Contact

Further information and requests for resources should be directed to and will be fulfilled by the Lead Contact, Joanna Slusky (slusky@ku.edu).

Data and materials availability

507 All strains used are commercially available. All plasmids available through Addgene. CryoEM
508 maps and models have been deposited with accession codes EMD-21960, EMD-21959, PDB ID
509 6WXI, and PDB ID 6WXH. All other data is available in the main text or the supplementary
510 materials.

511 **METHOD DETAILS**

512 ***E. coli* strains.** *E. coli* strains BW25113 and JW5503-1 were purchased from the Coli Genetic
513 Stock Center (CGSC). JW5503-1 is a *tolC732(del)::kan* from the parent strain BW25113.
514 BL21(DE3) were used for expression of the colicin constructs and TolC. BL21(DE3) has a
515 premature stop codon at residue 58 of the *btuB* gene and therefore we used it as a $\Delta btuB$ strain
516 for microscopy.

517
518 **Expression and Purification.** The gene for *colE1-TR* was synthesized as a gBlock (Integrated
519 DNA Technologies) and cloned into pET303. Inverse PCR was used to delete the R domain and
520 produce colicin E1-T. The gene for colicin E1-TR-GFP was produced by inserting GFP at the C
521 terminus of *colE1-TR*.

522
523 Plasmids were transformed into *E. coli* BL21(DE3) cells and plated on LB + agar + 100 $\mu\text{g}/\text{mL}$
524 carbenicillin. Single colonies were inoculated into 50 mL LB broth with 100 $\mu\text{g}/\text{mL}$ carbenicillin
525 and grown overnight at 37 °C with shaking at 250 r.p.m. Proteins were expressed by inoculating
526 1L of TB supplemented with 0.4% glycerol, 10 mM MgCl_2 and 100 $\mu\text{g}/\text{mL}$ carbenicillin with 20
527 mL of the overnight culture. The culture was grown at 37 °C to an OD600 of 2.0 and induced
528 with 1 mM IPTG. Expression cultures were then grown at 15 °C for 24 hours and harvested at
529 4,000 g for 30 minutes at 4 °C. Cell pellets were resuspended at 3 mL/g of cell pellet in lysis
530 buffer (TBS, 5 mM MgCl_2 , 10 mM imidazole, 1mM PMSF, 10 $\mu\text{g}/\text{mL}$ DNase, 0.25 mg/mL
531 lysozyme) and lysed via sonication (2 minutes, 2s on, 8s off, 40% amplitude, QSonica Q500
532 with 12.7 mm probe) in an ice bath. Lysates were centrifuged at 4,000 g for 10 minutes to
533 remove un-lysed cells and debris. The supernatant was centrifuged again at 50,400 g in a
534 Beckman Coulter J2-21 for 1 hour at 4 °C. Clarified lysates were applied to a 5 mL HisTrap FF
535 column and purified using an ÄKTA FPLC system with a 20 column volume wash step with
536 binding buffer (TBS, 25 mM imidazole) and eluted using a linear gradient from 0-50% elution
537 buffer (TBS, 500 mM imidazole) in 10 column volumes. Concentrated proteins were loaded onto
538 a HiLoad Superdex 16/60 200 pg gel filtration column and eluted into phosphate buffered saline
539 (PBS) pH 7.4.

540
541 TolC expression and purification was conducted in the same manner for preparation for cryoEM
542 and for SEC. The gene for full-length TolC (a generous gift from R. Misra) was cloned into
543 pTrc99a with the signal sequence deleted for expression into inclusion bodies. Plasmids were
544 transformed into BL21(DE3) and plated on LB + agar + 100 $\mu\text{g}/\text{mL}$ carbenicillin. A single
545 colony was picked and grown in LB at 37 °C with shaking at 250 r.p.m. overnight. In the
546 morning, 1L of LB was inoculated with 20 mL of the overnight culture and grown at 37 °C with
547 shaking at 250 r.p.m. until the culture reached an OD600 of 0.6, at which point protein
548 expression was induced with 1mM IPTG for an additional 4 hours. Cells were then harvested at
549 4,000g for 30 minutes at 4 °C. Cell pellets were resuspended in mL of lysis buffer (TBS, 5 mM
550 MgCl_2 , 0.2 mg/mL lysozyme, 5 $\mu\text{g}/\text{mL}$ DNase, 1mM PMSF) at 3 mL/1g of cell pellet and lysed
551 via sonication (4 minutes, 2s on, 8s off, 40% amplitude, QSonica Q500 with 12.7 mm probe) in
552 an ice bath. Cell lysates were centrifuged at 4,000 g for 30 minutes at 4 °C to harvest inclusion

553 bodies. Inclusion body pellets were resuspended in inclusion body wash buffer (20 mM Tris pH
554 8.0, 0.5 mM EDTA, 1% Triton X-100) and centrifuged at 4,000g for 30 minutes at 4 °C. The
555 inclusion body wash was repeated two more times. A final wash was done in 20 mM Tris pH 8.0
556 and inclusion bodies were stored at -20 °C. Inclusion bodies were solubilized in 20 mM Tris pH
557 8.0, 8M urea at 500 µM. N-octylpolyoxyethylene was added to 5 mL of solubilized TolC to a
558 final concentration of 10% detergent and pipetted into a Slide-A-Lyzer G2 dialysis cassette with
559 a 10,000 molecular weight cut off. Refolding was initiated by dialysis in 5L of 20 mM Tris pH
560 8.0, 100 mM NaCl at 4 °C with stirring overnight. TolC was centrifuged at 15,200 g for 10
561 minutes at 4 °C to remove aggregates. The supernatant was filtered through a 0.22 µm filter,
562 concentrated to 2 mL, applied onto a HiLoad 16/60 Superdex 200 pg column on an ÄKTA Pure
563 FPLC system, and eluted with 1.5 column volumes in 20 mM Tris pH 8.0, 100 mM NaCl, 0.05%
564 n-dodecyl-β-D-maltoside. TolC containing fractions were pooled and concentrated to 300 µM in
565 Amicon centrifugal filters with molecular weight cutoff of 30kDa.

566
567 Membrane scaffold protein MSP1D1. MSP1D1 in pET28a was purchased from Addgene and
568 was expressed and purified as previously described⁵⁶.

569
570 **Peptide Synthesis.** ColE1-T100-143 was synthesized using standard Fmoc chemistry with a
571 CEM liberty blue microwave peptide synthesizer. The peptides were cleaved using a solution of
572 92.5:2.5:2.5:2.5 TFA:TIPS:H₂O:DoDt and the crude peptides were purified using HPLC.
573 Analytical HPLC traces were acquired using an Agilent 1100 quaternary pump and a Hamilton
574 PRP-1 (polystyrene-divinylbenzene) reverse phase analytical column (7 µm particle size, 4 mm x
575 25 cm) with UV detection at 215 nm. The eluents were heated to 45 °C to reduce separation of
576 rotational isomers, and elution was achieved with gradients of water/ acetonitrile (90:10 to 0:100
577 containing 0.1% TFA) over 20 min. Low-resolution mass spectra (LRMS) were obtained using a
578 Waters Micromass ZQ 4000 instrument with ESI+ ionization

579
580 **Extracellular Protease Digestion.** Protein localization after exogenous protein addition to
581 whole cells was determined as previously described³⁸.

582
583 **Single-Molecule Microscopy.** Cysteine mutations were introduced at the C-terminus before the
584 histidine tag for fluorophore conjugation. These constructs were purified as described in the
585 expression and purification section with the addition of 1 mM TCEP in all buffers. All
586 subsequent steps were performed with limited exposure to light and in amber tubes. Cyanine3
587 (Cy3) maleimide (Lumiprobe) was reconstituted in DMSO. Fluorophore labeling was achieved
588 by mixing a 20-fold molar excess of Cy3 maleimide to protein and incubating overnight at 4 °C.
589 Free dye was removed by gel filtration on a Sephadex NAP-10 G-25 column. Simultaneously to
590 the dye removal, the sample was buffer exchanged into storage buffer (PBS pH 7.4, 1 mM DTT,
591 1 mM EDTA). The degree of labeling was determined spectrophotometrically from the
592 concentrations of the dye and protein solutions using their respective extinction coefficients, ε, as
593 described by their manufacturers or for the proteins as estimated by ExPASy ProtParam (Cy3
594 ε_{548nm} = 162,000 L mol⁻¹ cm⁻¹; colE1-T-E192C ε_{280nm} = 9,970 L mol⁻¹ cm⁻¹; colE1-TR-
595 E366C ε_{280nm} = 14,440 L mol⁻¹ cm⁻¹). Labeling efficiencies were ~75% and ~85% for colE1-
596 T-E192C and colE1-TR-E366C, respectively. Protein concentrations were adjusted according to
597 the percentage of labeled protein.

598

599 Cultures of *E. coli* (WT, Δ tolC, or BL21(DE3)) were grown in LB medium at 37 °C with
600 shaking (180 r.p.m.) overnight, then transferred to MOPS minimal medium (Teknova) with 0.2%
601 glycerol and 1.32 mM K_2HPO_4 , and grown at 37 °C for 13 h. The sample was transferred to
602 MOPS medium and grown to turbidity at 37 °C overnight. A 1-mL aliquot of culture was
603 centrifuged for 2 min at 4,850 g to pellet the cells. The pellet was washed in 1 mL MOPS and
604 centrifuged a second time. The supernatant was then removed, and the cell pellet was
605 resuspended in 500 μ L MOPS. A 1.0 μ L droplet of concentrated cells was placed onto a glass
606 slide. Then, a 1.0 μ L droplet of 1 μ g/mL colicin E1 protein construct stock was added to the
607 cells. The droplet was covered by an agarose pad (1% agarose in MOPS media) and a second
608 coverslip.

609
610 Samples were imaged at room temperature using wide-field epifluorescence microscopy with
611 sensitivity to detect single dye molecules as described previously³⁹. Briefly, fluorescence was
612 excited by a 561-nm laser (Coherent Sapphire 560-50) for Cy3 or a 488-nm laser (Coherent
613 Sapphire 488-50) for GFP. The lasers were operated at low power densities (1 – 2 W/cm²), and
614 fluorescence was imaged with an Olympus IX71 inverted microscope with a 100x, 1.40-NA oil-
615 immersion objective and appropriate excitation, emission, and dichroic filters. A Photometrics
616 Evolve electron multiplying charge-coupled device (EMCCD) camera with > 90% quantum
617 efficiency captured the images at a rate of 20 frames per second. Each detector pixel corresponds
618 to a 49 nm \times 49 nm area of the sample.

619
620 **Co-elution.** The interaction of TolC and colicin E1-T or -TR were determined by co-elution on
621 an SEC column. Purified TolC and colicin E1-T or -TR were mixed at a 1:2 molar ratio and
622 incubated at room temperature for 1 hour before loading onto a Superdex 200 Increase 10/300
623 GL column (GE Healthcare). The protein was eluted with 1.5 column volumes into 20 mM Tris
624 pH 8.0, 40 mM NaCl, 0.05% n-dodecyl- β -D-maltoside for colE1-T. For colE1-TR the NaCl
625 concentration was increased to 200 mM to prevent precipitation. Elution fractions were collected
626 every 0.5 mL. Peak fractions were concentrated to 20 μ L and analyzed by 4-20% SDS-PAGE.

627
628 **Real-Time Efflux.** Real-time efflux activity in the presence of colE1-TR was determined as
629 previously described with some modifications^{46,47}. Cells were resuspended to OD₆₀₀ 1.5 in cold
630 PBS with and without 10-100 μ M colicin proteins and incubated for 15 minutes on ice. To turn
631 off efflux, 100 μ M carbonyl cyanide m-chlorophenyl hydrazone (CCCP) was added. After an
632 additional 15 minutes the efflux dye NNN was added to the cells to 10 μ M. The cells were
633 incubated at 25 °C with shaking at 140 r.p.m. for 2 hours. Cells were harvested at 3,500 g for 5
634 minutes and washed once in 20 mM potassium phosphate buffer pH 7 with 1mM $MgCl_2$. Cell
635 concentrations were adjusted to OD₆₀₀ 1.0 and placed on ice. Then, 2 mL of the cell suspension
636 was loaded into a quartz cuvette (Agilent Technologies). Fluorescence was measured with an
637 Agilent Cary Eclipse fluorescence spectrophotometer with slit widths at 5 and 10 nm for
638 excitation wavelength of 370 nm and emission wavelength of 415 nm. Fluorescence
639 measurements were taken every 1 second. After 100 seconds, 50 mM glucose was added to re-
640 energize the cells and initiate efflux, and fluorescence data were collected for an additional 600
641 seconds.

642
643 **Minimum Inhibitory Concentrations (MICs).** MICs were determined using the broth dilution
644 method⁵⁷ with some modifications in 96 well plate format using LB media in 100 μ L well

645 volumes. Cultures were grown at 37 °C with shaking at 250 r.p.m. and OD600 was read on a
646 Biotek plate reader after 20 hours. MICs are defined by the lowest concentration that prevents
647 visible growth. We chose an OD600 of >0.1 as the cutoff for growth. We report MICs as the
648 mean of 3 or 6 biological replicates with each replicate plotted (Figure 3D, Table S2). Due to the
649 2-fold discretized nature of concentration ranges used to determine MICs we do not report
650 statistical significance values as is typical of MIC reporting.

651
652 **Reconstitution of TolC into Amphipol.** Amphipol A8-35 (Anatrace) was solubilized in water at
653 33 mgs/mL. 1 mL of TolC at 0.5 mg/mL was mixed with 0.75 μ L of A8-35 at 33 mg/mL for a 5-
654 fold weight excess and incubated at room temperature for 30 minutes. Bio-Beads SM-2 resin that
655 was washed in methanol and equilibrated with 20 mM Tris, 40 mM NaCl was added to the
656 reaction mixture at 0.5 g/mL to initiate detergent exchange for A8-35 and incubated with rotation
657 at 4 °C overnight. The mixture was transferred to a tube with fresh Bio-Beads and incubated at 4
658 °C for an additional 4 hours. The reaction mixture was loaded onto a HiLoad 16/60 Superdex
659 200 pg column on an ÄKTA Pure FPLC system and eluted with 1.5 column volumes in 20 mM
660 Tris pH 8.0, 40 mM NaCl to remove free A8-35 and detergent. For colicin-bound TolC in A8-35,
661 colicin E1-T was added to the reaction mixture at a >2 molar excess prior to gel filtration. TolC
662 or colicin-bound TolC in A8-35 was concentrated to 2-4 mg/mL for cryoEM.

663
664 **Reconstitution of TolC into lipid nanodiscs.** POPC (Avanti Polar Lipids) in chloroform was
665 dried under a stream of nitrogen and freeze dried to remove residual chloroform. Lipids were
666 reconstituted to 50 mM in cholate buffer (20 mM Tris pH 8.0, 100 mM NaCl, 0.5 mM EDTA,
667 100 mM cholate) in an amber glass vial. The vial was submerged under a stream of warm water
668 until the solution became clear. Lipids, membrane scaffold protein, and TolC were mixed in a
669 36:1:0.4 ratio as previously described⁵⁸. Final concentrations were 4.5 mM POPC, 125 μ M
670 MSP1D1, 50 μ M TolC in a 2 mL reaction with cholate brought up to 20 mM and dodecyl-
671 maltoside up to 0.1%. The reaction mixture was incubated on ice for 1 hour. Bio-Beads SM-2
672 resin that was washed in methanol and equilibrated with 20 mM Tris, 40 mM NaCl were added
673 to the reaction mixture at 0.5 g/mL to initiate nanodisc formation and incubated with rotation at
674 4°C overnight. The mixture was transferred to a tube with fresh Bio-Beads and incubated at 4 °C
675 for an additional 4 hours. The reaction mixture was loaded onto a HiLoad 16/60 Superdex 200
676 pg column on an ÄKTA Pure FPLC system and eluted with 1.5 column volumes in 20 mM Tris
677 pH 8.0, 40 mM NaCl to separate TolC inserted into nanodiscs from empty nanodiscs. For
678 colicin-bound TolC in nanodiscs, colicin E1-T was added to the reaction mixture at a >2 molar
679 excess prior to gel filtration. TolC or colicin-bound TolC in nanodiscs was concentrated to 2-4
680 mg/mL for cryoEM.

681
682 **Cryoelectron microscopy.** 3 μ L of protein solution (TolC/colE1-T in amphipol or TolC/colE1-T
683 in nanodiscs) was diluted to approximately 1.05 mg/mL concentration, applied to a glow-
684 discharged TEM grid, and plunge-frozen in ethane using a Vitrobot Mark IV (FEI Company)
685 with grade 595 filter paper (Ted Pella). Glow discharge was performed in ambient atmosphere at
686 0.39 mBar pressure. Imaging was performed using a Talos Arctica (FEI Company) operated at
687 200 kV with energy-filter and K2 Summit (Gatan, Inc.) for detection. To collect multiple images
688 per hole while maintaining parallel illumination conditions, a nonstandard 20 μ m condenser
689 aperture was used to image TolC-colE1-T in nanodiscs. At nominal magnification of 205,000 \times ,
690 images were acquired in counting mode with a calibrated pixel size of 0.6578 Å. Fresnel fringes

691 attributable to the beam interaction with the aperture were often seen in images. Some
692 investigators have moved the microscope stage and altered the nominal objective lens true focus
693 point to generate a fringe-free condition⁵⁹. In this study, imaging at 205,000× with a 20 μm
694 aperture yielded better results than imaging at 130,000× with a 50 μm aperture; at 130,000× with
695 a 20 μm aperture the fringes were extremely severe due to the larger field of view, so a full
696 dataset was not collected with those conditions. TolC in nanodiscs (without colE1-T) was
697 imaged at 130,000× with a 50μm condenser aperture (Table S1).

698
699 Micrographs were collected with SerialEM⁶⁰ using in-house modifications of the scripts of Chen
700 Xu (sphinx-emdocs.readthedocs.io). Briefly, multishot imaging was configured with 4 images
701 per hole for each of 16 holes; intermediate-magnification montages of grid squares were
702 acquired; points were selected manually for collection of 64 images per point; images were
703 acquired using coma-compensated image shift as gain- and dark-corrected LZW-compressed
704 TIFs. Side, top, and oblique views were seen in areas of thin ice. During screening, ice thickness
705 was estimated at 17-30nm by the method of I_0/I_{ZLP} ⁶¹.

706
707 The collection of micrographs of TolC without colicin at 130,000× magnification has been
708 previously described⁶².

709
710 **3D reconstruction and modeling.** Final reconstructions were obtained using cryoSPARC 2⁶³.
711 1,018 micrographs were collected of amphipol-embedded TolC/colE1-T. Micrographs were
712 motion-corrected using RELION 3⁶⁴. CTF parameters were determined by means of *ctffind*⁶⁵.
713 115,362 particles were selected with crYOLO⁶⁶. 2D classification revealed that many particles
714 had aberrant morphology and only 24,624 (21%) were selected for 3D reconstruction. *Ab initio*
715 reconstruction in cryoSPARC 2⁶³ was effective at recovering a map whose shape was similar to
716 that of previously described TolC trimers. However, the data could only be refined to a nominal
717 global resolution of 6.0 Å, and luminal density was insufficiently resolved. 4,492 micrographs
718 were then collected of nanodisc-embedded TolC/colE1-T and processed similarly. Of the
719 339,779 particles detected by cryoSPARC Live, 179,834 (53%) were in good classes. Although
720 there were slightly fewer particles per micrograph in the nanodisc dataset, more particles per
721 micrograph were usable. Beginning with the *ab initio* model and mask derived from the
722 amphipol data, this particle set was refined by cryoSPARC 2 non-uniform refinement with or
723 without imposed C_3 symmetry. The maps refined to nominal global resolutions of 2.81 Å and
724 3.09 Å for the symmetrized and asymmetric maps, respectively. There was local variation in
725 resolution within the map, with consistent, high resolution in the middle of TolC and lower
726 resolution at the lids and for colE1-T. Local resolution was computed in cryoSPARC by the
727 locally windowed FSC method⁶⁷ and rendered with UCSF Chimera. To reduce the voxel-based
728 values to averages for four regions of the complex, the local resolution map was masked to
729 include only voxels within 3 Å of a modeled atom and then the median value was calculated for
730 those voxels closest to colE1, closest to TolC residues 168-172 and 386-390, closest to TolC
731 residues 285-301 and 76-82, or closest to other TolC residues. Furthermore, it is notable that
732 while the nanodisc appears as a double-belt in the symmetrized map, in the asymmetric map the
733 nanodisc protein mostly appears on the side of TolC that is bound to colE1-T. One possible
734 explanation is that, despite masking, nanodisc asymmetry is a confounder of the asymmetric
735 refinement and is one source of heterogeneity in the data. Another possibility is that the C-

736 terminus of colE1-T forms an interaction with the nanodisc, causing preferential alignment of the
737 nanodisc with respect to the TolC/colE1-T complex.

738
739 196,158 particles of TolC without colicin were obtained as previously described⁶².
740 Homogeneous refinement yielded a structure at 2.89 Å; local motion correction and global CTF
741 refinement yielded a final map at 2.84 Å.

742
743 Modeling was initiated by rigidly docking a crystal structure of TolC in complex with
744 hexammincobalt (1TQQ)³⁰ into the symmetrized map density. Automated, semi-automated, and
745 manual real-space refinement was performed using phenix⁶⁸, ISOLDE⁶⁹, and coot⁷⁰. For TolC
746 with colE1-T, additional refinement was performed in AMBER using the cryoEM density map
747 as a restraint.

748
749 Although additional residues are present at the TolC C-terminus, these were not modeled
750 because the density becomes unsharp after residue 428. Blurred density in the map suggests that
751 the C-terminus follows helix 3 towards the periplasmic end of the molecule. ColE1-T was
752 modeled *ab initio*. The 3-fold symmetrized map contains density at ~1/3rd occupancy for colE1-T
753 and this density contains some high-resolution information not present in the asymmetric map,
754 except near the TolC lid regions where symmetrization overlays colE1-T density with TolC
755 density at a threefold-related position. First, polyalanine helices were placed in the helical
756 density in coot. Cross-correlation coefficients for both helices are higher with the N-terminus
757 oriented towards the periplasm, and the Christmas tree appearance was observed indicating that
758 this is the correct chain orientation. An estimate of the registration was made by visual inspection
759 of potential anchor residues. Finally, the hinge region was filled in using phenix and coot. This
760 completed chain was refined against the asymmetric map in ISOLDE. Iteration between phenix,
761 coot, and ISOLDE was continued until acceptable fit to density was achieved. In the case of
762 TolC with colE1-T, the map was further improved by combining map information with
763 molecular dynamics force fields³³. Briefly, starting with the phenix/coot/ISOLDE-refined model,
764 we performed restrained simulated annealing in AMBER, heating from 0K to 300K for 0.2 nsec,
765 holding constant temperature for 1 nsec, and then cooling to 0K over 0.2 nsec. The cryoEM
766 density map is utilized as a restraint potential in the annealing so that both map information and
767 AMBER force field information are simultaneously utilized to obtain an optimum model
768 consistent with the data³³. The protein force field used the ff14SB force field⁷¹ and a generalized
769 Born implicit solvent model with $igb=8$ ⁷², and a nonbonded cutoff of 20 Å. The relative weight
770 of real-space map-based restraints and the force field was fixed using $fcons=0.02$. For colE1-T,
771 information from the symmetrized map was integrated into the modeling procedure during
772 manual remodeling in coot, but map-based refinement in phenix, ISOLDE, and AMBER were
773 against the asymmetric map. TolC without colE1-T was modeled similarly but using the TolC-
774 colE1-T structure as a starting point instead of 1TQQ, and without final AMBER refinement.

775
776 Molecular representations were generated with Chimera, ChimeraX⁷³ or PyMOL (Schrödinger,
777 LLC).

778

779

780

Supplemental Information

781

782

783

Colicin E1 binds to TolC as an open hinge to penetrate the outer-membrane

784

785

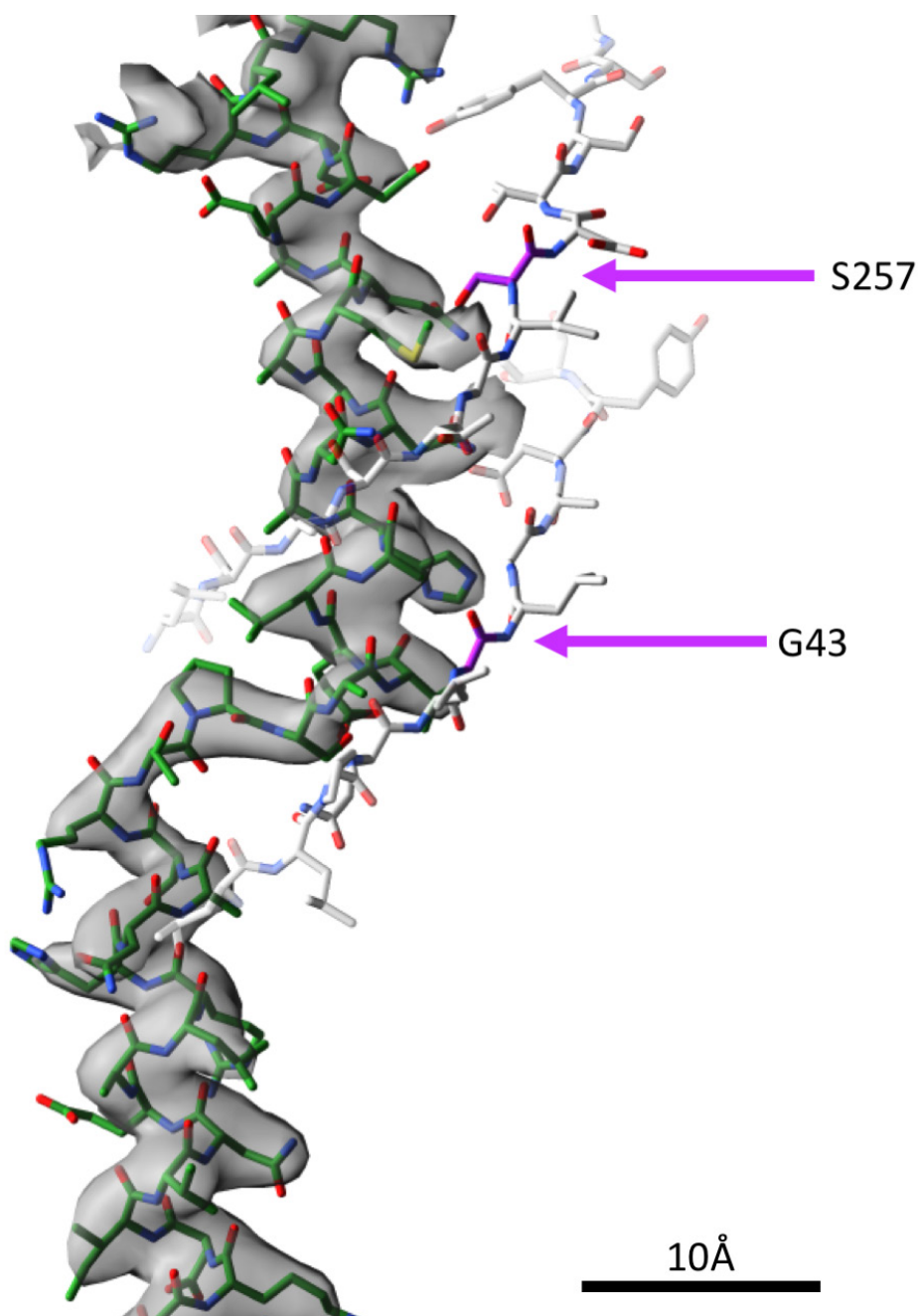
S. Jimmy Budiardjo, Jacqueline J. Stevens, Anna L. Calkins, Ayotunde P. Ikujuni, Virangika K.

786

Wimalasena, Emre Firlar, David A. Case, Julie S. Biteen, Jason T. Kaelber and Joanna S.G.

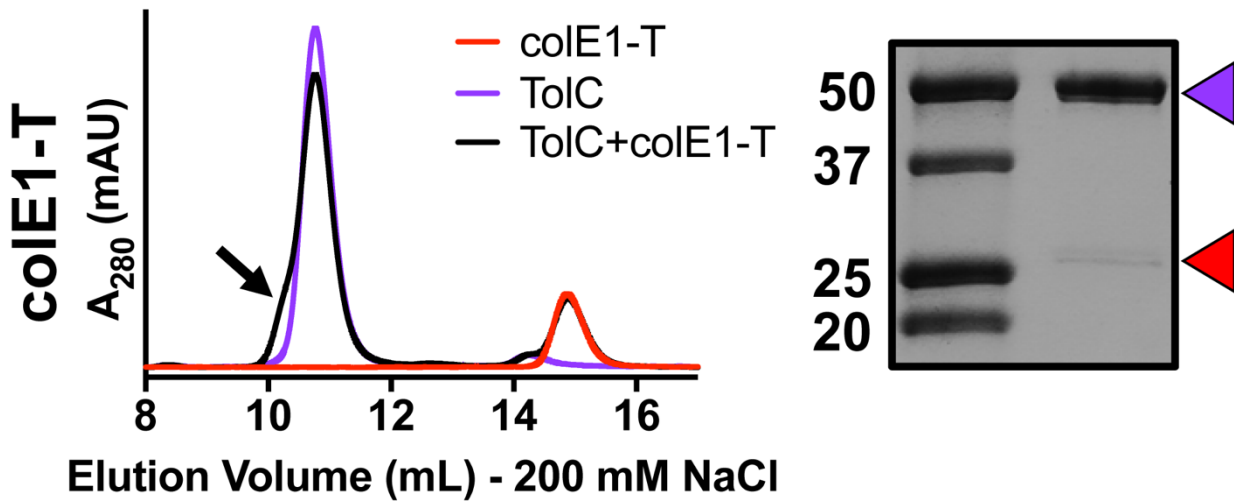
787

Slusky



788
789
790
791
792
793
794
795

Figure S1. TolC box density cropped from the fully asymmetric cryoEM map of the TolC/colE1-T complex. Mutations at positions G43 and S257 in the TolC (grey sticks) barrel make direct contact with colE1-T (green). These mutations were previously shown to abolish WT colE1 function³⁶. Mutations to bulkier side chains introduce a steric clash that prevents binding.

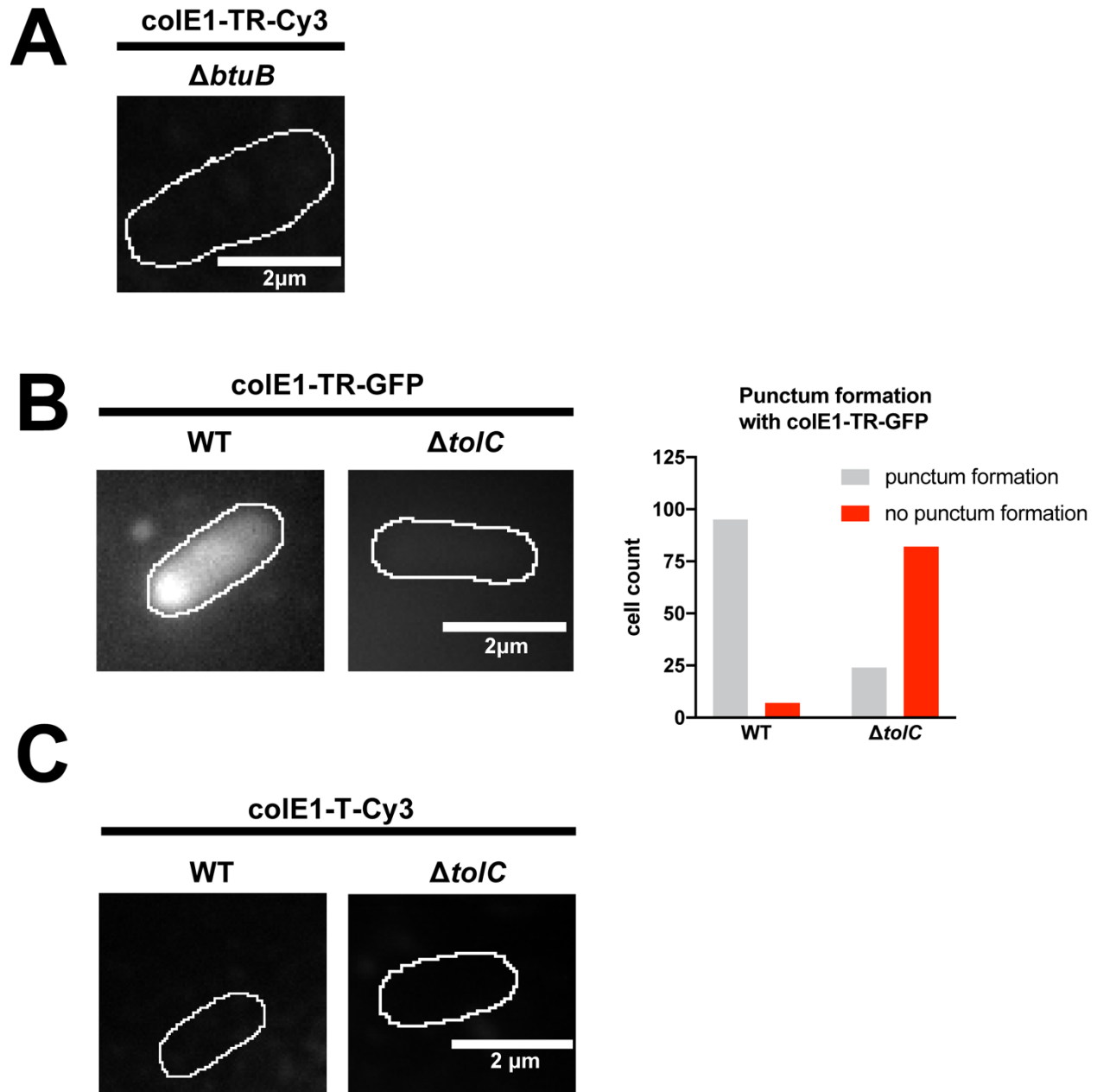


796

797 **Figure S2. Co-elution of colE1-T with TolC at 200 mM NaCl (black).** Under this higher salt
798 concentration, when TolC (purple) and colE1-T (red) are mixed, there is a smaller peak shift than
799 that seen with colE1-TR and the presence of a shoulder (black arrow). SDS-PAGE of the
800 shoulder shows presence of both TolC (purple arrow) and colE1-T (red arrow). Although some
801 binding was detected, this higher salt concentration prevents full binding as indicated by a much
802 fainter band for colE1-T than seen at the lower salt concentration (Figure 4A).

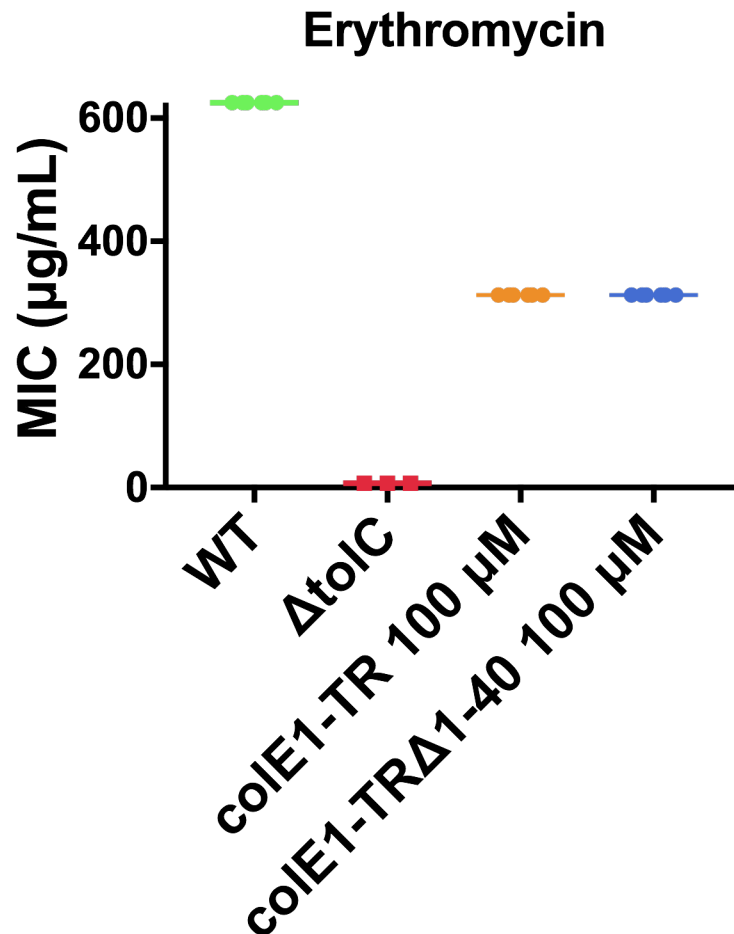
803

804



805
806 **Figure S3 Single-molecule microscopy.** Fluorescence images overlaid on outlines of living *E.*
807 *coli* cells from phase-contrast microscopy for WT and $\Delta tolC$ for colE1-TR-GFP and counts of
808 cells where colE1-TR-GFP punctum formation was observed. (A) 97% of cells showed no
809 binding of Cy3-labeled colE1-TR to $\Delta btuB$ (B) ColE1-TR-GFP forms similar puncta as Cy3-
810 labeled ColE1-TR (main text Figure 4C). (C) No binding of Cy3-labeled colE1-T to WT or
811 $\Delta tolC$ cells was detected with Cy3-labeled colE1-T. Scale bars: 2 μ m.
812
813
814
815
816
817

818
819



820

821

822 **Figure S4. Minimum Inhibitory Concentration of Erythromycin with colE1-TR TolA box**
823 **deletion construct.** The MIC for erythromycin with 100 μM colE1-TR or colE1-TR_{Δ1-40} is
824 identical indicating that TolA engagement by colE1-TR does not contribute to antibiotic
825 susceptibility.

826

827

828

829

830 **Table S1**
 831 Cryo-EM data collection, refinement, and validation statistics

832

	TolC (EMDB-21960) (PDB 6WXI)	TolC + colE1 (EMDB-21959) (PDB 6WXH)
Data collection and processing		
Electron microscope	Talos Arctica	Talos Arctica
Magnification	130,000×	205,000×
Voltage (kV)	200	200
Electron exposure (e-/Å ²)	33.04	35.96
Defocus range (μm)	0.5-2.6	0.4-2.1
Pixel size (Å)	1.038	0.6578
Symmetry imposed	C ₃	C ₁ (C ₃)
Initial particle images (no.)	2,092,678	339,779
Final particle images (no.)	778,220	179,834
Map resolution (Å)	2.84	3.09 (2.81)
FSC threshold	0.143	0.143
Refinement		
Initial model used (PDB code)	6WXH	1TQQ
Model resolution (Å)	3.11	3.37
FSC threshold	0.5	0.5
R.m.s. deviations		
Bond lengths (Å)	0.0072	0.012
Bond angles (°)	1.11	1.76
Validation		
MolProbity score	1.33	0.50
Clashscore	4.42	0.00
Poor rotamers (%)	1.40	0.18
Ramachandran plot		
Favored (%)	98.12	98.31
Allowed (%)	1.88	1.32
Disallowed (%)	0	0.37

833

834

835 **Table S2.**
836 Mean minimum inhibitory concentrations (MICs) of antimicrobials in the presence of colE1-TR.

837

	Erythromycin ($\mu\text{g/mL}$)	Ciprofloxacin (ng/mL)	Kanamycin ($\mu\text{g/mL}$)	Benzalkonium Chloride ($\mu\text{g/mL}$)
WT	625.00	56.25	21.88	45.83
<i>ΔtolC</i>	7.03	15.63	NA	6.88
WT + 10 μM colE1-TR	364.58	75.00	28.14	25
WT + 100 μM colE1-TR	312.50	28.13	6.25	6.25

838

839

840
841
842
843
844
845
846

Movie S1.

A representative 8-second clip of colE1-TR bound to a live cell. ColE1-TR localizes on, and remains bound to, the extracellular surface of *E. coli*. Fluorescence movie of Cy3-labeled colE1-TR on living WT *E. coli* overlaid on outline of the *E. coli* cell from phase-contrast microscopy. Continuous imaging at 25 frames per second. Scale bar: 2 μm .